Interpretation of the Electronic Spectra of Four Disilanes†

Mari Carmen Piqueras,‡ Raül Crespo,*,‡ and Josef Michl*,§,||

Departament de Química Física, Universitat de València, Dr. Moliner 50, E-46100 Burjassot, Spain, Department of Chemistry and Biochemistry, University of Colorado, Boulder, Colorado 80309-0215, and Institute of Organic Chemistry and Biochemistry, Academy of Sciences of the Czech Republic, Flemingovo nám. 2, 18200 Prague 8, Czech Republic

Received: May 27, 2008; Revised Manuscript Received: August 7, 2008

Time-dependent density functional theory (TD-DFT/B3LYP(AC)/cc-pVTZ/cc-pVTZ/6-311G//MP2/cc-pVTZ/cc-pVTZ/6-31G**) has been used to compute vertical excitation energies and oscillator strengths of the six low-lying excited states of four peralkylated disilanes, hexamethyldisilane (**1**), hexa-*tert*-butyldisilane (**2**), 1,6-disila[4.4.4]propellane (**3**), and 1,7-disila[5.5.5]propellane (**4**). The results provide an accurate interpretation of the reported UV absorption spectra of **1**−**4** in solution, and for **1** also in the gas phase up to 62 000 cm^{-1}. The excellent agreement of the calculated with the available experimental energies and oscillator strengths, and with magnetic circular (MCD) and linear (LD) dichroism, gives us confidence that the method will be useful for dependable interpretation of the electronic spectra of longer oligosilanes. Although the disilane chromophore finds itself in quite different environments in **1**−**4**, its fundamental characteristics remain the same, with one important exception. In all four compounds, the first valence excited state is due to an electron promotion from the σ_1 HOMO to the π_1* orbital, and the second valence excited state to a promotion from the σ_1 HOMO to the σ_1* orbital. Surprisingly, however, it is only in **2**, which has an extraordinarily long SiSi bond, that the terminating σ_1* orbital is the σ*(SiSi) antibond, as anticipated, and the $\sigma\sigma$* transition has the expected very high oscillator strength. In **1**, **3**, and **4**, the σ*(SiSi) antibonding orbital is high in energy and does not play any role in low-energy excitations. Instead, the terminating orbital of the $\sigma_1\sigma_1$* excitation is represented by Si−alkyl antibonds, combined symmetrically with respect to rotation around the SiSi axis and antisymmetrically with respect to operations that interchange the two Si atoms. The common assumption that the characteristic intense $\sigma\sigma$* transitions of longer peralkylated oligosilanes extrapolate to the lowest $\sigma\sigma$* transition in common peralkylated disilanes is incorrect, and only the weak $\sigma\pi$* transitions extrapolate simply.

Introduction

Potential industrial applications and new properties of peralkylated polysilanes and oligosilanes have attracted many experimental and theoretical studies.[1] These stable compounds display unique optical features in the near UV region attributed to σ-electron delocalization and represent a prime example of σ-conjugated systems. The resolution of the densely spaced excited states of these fascinating conjugated systems represents a considerable challenge. With the exception of disilane and trisilane, linear oligosilanes are normally present as complex mixtures of rapidly interconverting conformers, each of which has its own distinct spectral properties. Furthermore, the valence excited states of oligosilanes occur at energies that are not far separated from the lowest Rydberg states.[2,3] Both absorption and emission bands are broad and featureless. Because of all of these difficulties, and after considerable effort, among the longer chains only the peralkylated tetrasilane chromophore is understood in detail as a function of the backbone dihedral angle, with several of the expected transitions to valence excited states identified.[4−7]

The Si−Si single bond is the fundamental constituent unit of all oligosilanes and polysilanes, and it can be viewed as a model for a general study of electronic states of σ bond systems. An understanding of the peralkylated disilane chromophore is likely to play an essential role in any effort to interpret σ excited states of longer peralkylated oligosilane chains. Among peralkylated disilanes, hexamethyldisilane (**1**, Chart 1) is the simplest compound containing the disilane chromophore and has been the most widely studied. The UV absorption spectrum of this compound has been measured[8−12] and calculated.[13,14] The next member of the peralkyldisilane series, hexaethyldisi-

CHART 1

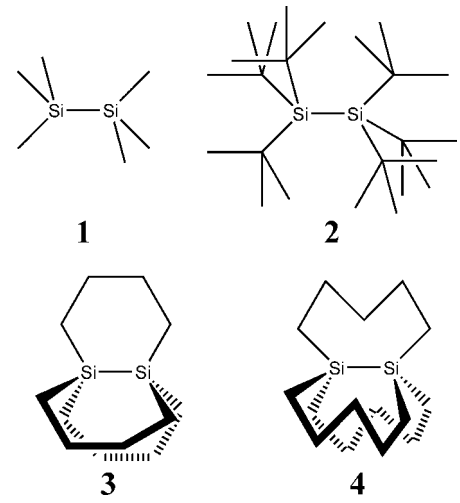

† Part of the "Sason S. Shaik Festschrift".

* To whom correspondence should be addressed. E-mail: raul.crespo@uv.es (R.C.), michl@eefus.colorado.edu (J.M.).

‡ Universitat de València.

§ University of Colorado.

|| Academy of Sciences of the Czech Republic.

10.1021/jp804677v CCC: $40.75
Published on Web 09/27/2008

lane, does not display any striking features,[12] but hexa-*tert*-butyldisilane (**2**, Chart 1)[15] does. Its UV absorption spectrum is distinctly red-shifted from that of **1**, and this has been attributed to its unusually long Si−Si bond,[15] relative to **1**.[16] The UV, LD, and MCD spectra of **2** have been published,[12] together with the spectra of an unusual tricyclic disilane, 1,6-disila[4.4.4]propellane (**3**, Chart 1), which has a quite short Si−Si bond,[17] and whose first UV absorption maximum is also significantly red-shifted with respect to that of **1**.[8] The UV and MCD spectra of a related compound, 1,7-disila[5.5.5]propellane (**4**, Chart 1), whose Si−Si bond distance is intermediate between those of **1** and **3**, were also included.[12] These four distinct disilanes contain the disilane chromophore in very different environments, with bond lengths ranging from 2.295 Å (**3**) to 2.686 Å (**2**). They therefore represent an especially suitable set for a study of the disilane chromophore.

Previous density functional theory computations accounted only qualitatively for the spectral features displayed by the four compounds **1**−**4**. The assignment and characterization of the lowest observed UV transitions to valence excitations of $\sigma\pi^*$ or $\sigma\sigma^*$ character and the relative intensity of these transitions were the main focus.[12] These two types of transitions are well defined by symmetry in disilanes and in those oligosilanes that have a planar silicon backbone. Both involve excitation from high-lying σ molecular orbitals composed of SiSi bond orbitals. The highest occupied molecular orbital (HOMO) is of this type. In transitions of the $\sigma\pi^*$ type, the electron is promoted into a molecular orbital that is antisymmetric with respect to the backbone plane and is composed of out-of-phase combinations of SiC antibond orbitals, that is, contains contributions from Si(3p) atomic orbitals whose axis is perpendicular to the backbone plane. In the shortest oligosilanes, the lowest unoccupied molecular orbital (LUMO) is of this type. In transitions of the $\sigma\sigma^*$ type, the promotion is into a molecular orbital that is symmetric with respect to the backbone plane and is composed of SiSi antibond orbitals. This orbital is the LUMO in all except the shortest oligosilanes.

In oligosilanes with a nonplanar silicon backbone, orbitals of the σ and π types can no longer be rigorously distinguished, but in many cases the distinction between the two types of excitation can still be made approximately and remains useful. Some of the complexity of conformational effects on the spectra of oligosilanes is due to the avoided crossing of zero-order $\sigma\pi^*$ and $\sigma\sigma^*$ states as dihedral angles change.[3−7]

In trisilanes and higher oligosilanes, $\sigma\pi^*$ transitions are weak and hard to detect. The lowest one has been proposed to play an essential role in the unusual "inverse" thermochromic effect in the shortest oligosilanes, especially in trisilane,[14,18] and more than one have been identified and assigned in tetrasilanes.[3−7] In contrast, the very intense first $\sigma\sigma^*$ (HOMO to LUMO) transition is easy to detect and is the most characteristic of oligosilanes and polysilanes. Frequently, it is the only one discussed.

Liu et al.[13] used density functional theory (DFT) with local density approximation (LDA) to calculate the optical absorption spectra of permethylated oligosilanes as a function of their backbone chain length. The results showed correctly the variation of the excitation energy as a function of chain length in a series of all-*anti* conformers, including **1**, but the values were all about 1.0 eV too low. A later attempt to describe the first absorption band of the UV spectrum of all-*transoid* permethyloligosilanes Si_nMe_{2n+2} ($n = 2-8$, 10)[14] using time-dependent density functional theory (TD-B3LYP/6-311G(d,p)), also including **1**, resulted in energy values that agreed better but were about 0.25 eV too high, and in oscillator strength values that were also too low.

To date, DFT studies of oligosilanes did not give highly accurate values for the excitation energies or oscillator strengths, and this has hindered the definitive assignment of the electronic transitions. As a consequence, there are still some open questions about the assignment of the observed UV absorption bands to the different types of electronic transitions, the position of the Rydberg states, the behavior of the oscillator strengths as a function of the Si−Si bond length, etc. We have now characterized the low-lying excited states of **1**−**4** using an advanced TD-DFT method with the asymptotic correction approach of Casida and Salahub.[19]

A full theoretical description of the spectra of these systems is of value both in itself and as an assessment of the ability of current computational methods to handle σ-conjugated silicon containing systems. The nature of the excited states of oligosilanes makes an accurate treatment particularly challenging, because computations usually need to deal with large numbers of states of similar energy, making the separation of the valence and Rydberg bands quite difficult. The TD-DFT method used in this Article gives accurate values for both energies and oscillator strengths and holds promise for longer oligosilanes.

Computational Details

Optimized geometries were obtained using second-order Møller−Plesset perturbation theory (MP2) as implemented in the Gaussian 03 program.[20] They were started at the MP2/6-31G* level, and frequency analyses were performed at this level. They revealed the equilibrium geometry to be of D_{3d} symmetry for **1**, D_3 for **2** and **3**, and C_3 for **4**. This was followed by further optimizations at the MP2 level employing Dunning's correlation consistent triple-ζ basis set (cc-pVTZ)[21] on Si and C atoms and Pople's 6-31G** basis set[22] on H atoms, assuming the above symmetries. In all systems, the two silicon atoms were located on the z axis.

Electronic properties were computed at the TD-DFT level using the B3LYP functional.[23] The calculations were carried out on the MP2 optimized geometry with the cc-pVTZ basis set[21] for silicon and carbon atoms and the 6-311G basis set[24] for the hydrogen atoms, and used the asymptotic correction approach of Casida and Salahub[19] combined with the phenomenological linear correlation of Zhan, Nichols, and Dixon[25,26] as implemented in the NWChem program.[27]

This method of calculation was chosen because it gave good results in our previous paper on electronic excitation in a *syn*-tetrasilane.[28] It rectifies the problem of the breakdown of TD-DFT for high-lying excited states because of the incorrect asymptotic behavior of most of the exchange-correlation potentials. This asymptotic correction scheme combined with the B3LYP functional [B3LYP(AC)] has been shown to be well balanced for both valence and Rydberg transitions, giving improved excitation energies with respect to uncorrected B3LYP TD-DFT.[26] To gain assurance that the nature of the lowest σ^* orbital in **1** was independent of the basis set choice, the DFT/B3LYP calculations were repeated with the 6-31G*, 6-311G**, cc-pVTZ/cc-pVTZ/6-311G, cc-pVTZ, basis sets using the Gaussian 03 program, and both with and without the asymptotic correction with the 6-31G** and cc-pVTZ/cc-pVTZ/6-311G basis sets using the NWChem program.

Results

Optimized Geometries. The optimized Si−Si and Si−C bond lengths and SiSiC bond angles calculated at the MP2/cc-

TABLE 1: Observed and MP2/cc-pVTZ/cc-pVTZ/6-31G Optimized Geometrical Parameters of Disilanes 1−4**

	experimental			calculated		
compd	Si−Si	Si−C	SiSiC	Si−Si	Si−C	SiSiC
1 (D_{3d})	2.340[a]	1.877[a]	108.4[a]	2.356	1.892	110.11
2 (D_3)	2.686[b]	1.992[b]	111.71[b]	2.667	1.988	111.84
3 (D_3)	2.295[c]	1.893[d]	105.9[c]	2.301	1.897	105.76
4 (C_3)				2.322	1.894	110.26

[a] From ref 16. [b] From ref 15. [c] From ref 17. [d] From ref 29.

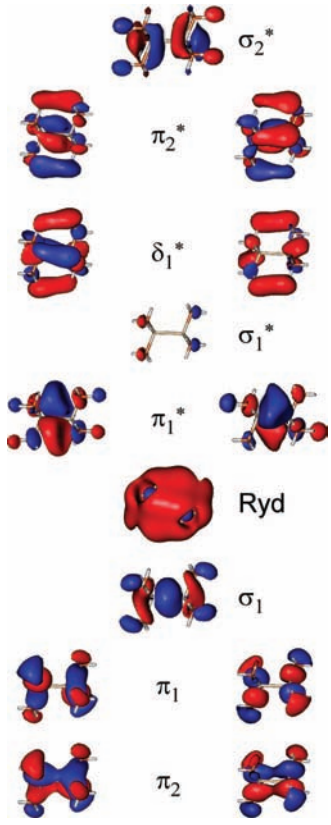

Figure 1. DFT orbitals for hexamethyldisilane (**1**). The isodensity surface value is 0.03, except for the Rydberg orbital, for which it is 0.012.

pVTZ/cc-pVTZ/6-31G** level are listed in Table 1, together with available experimental data.[15−17,29] The calculated Si−Si bond distance is 2.356 Å for **1** and is shorter in the propellanes, 2.301 Å in **3** and 2.322 Å in **4**. A much longer bond, 2.667 Å, is calculated for **2**. All Si−C bonds fall into a narrow range between 1.892 and 1.897 Å except for those in **2**, which show a distinctly larger value of 1.988 Å. Similarly, C−C bonds in **2**−**4** range only from 1.533 to 1.541 Å. SiSiC bond angle values are calculated to be around 110−112° except for **3** (105.8°).

In **1**, the Si−C bonds on the two silicon atoms are staggered. In **2**, they are approximately staggered, while in **3** and **4** they are approximately and perfectly eclipsed, respectively.

Orbitals. Figure 1 shows the Kohn−Sham orbitals obtained for **1** at the DFT/B3LYP(AC) level. The HOMO (symmetry a_{1g}) is a σ orbital (σ_1), and the HOMO−1 (symmetry e_g) and the HOMO−2 (symmetry e_u) are of the π type (π_1 and π_2, respectively) and correspond closely to simple Hückel expectations for σ(SiSi) and π(SiC) bond orbitals. For all other systems, the five highest occupied orbitals show the same features and have the symmetry of the irreducible representation of the corresponding symmetry group (a_1 and e for D_3 and a and e for C_3).

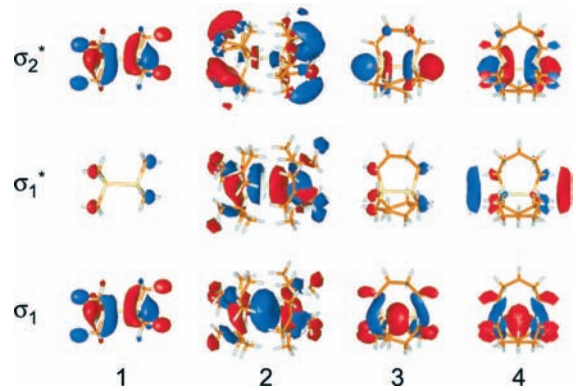

Figure 2. DFT orbitals for disilanes **1**−**4**. The isodensity surface value is 0.03 for **1** and **4**, 0.02 for **2**, and 0.04 for **3**.

The virtual orbitals of all systems also show the same characteristics, but their energy order is not the same in each molecule. In **1**, the LUMO (symmetry a_{1g}) is a Rydberg orbital. The LUMO+1 and LUMO+4 (symmetry e_u) are of the π* type (π_1* and π_2*, respectively). The LUMO+2 and LUMO+5 (symmetry a_{2u}) MOs are of the σ* type and correspond to the σ_1*(SiC) and σ_2*(SiSi) bond orbitals, respectively. The LUMO+3 (symmetry e_g) is of δ type (δ_1*).

In **2**, the LUMO (symmetry a_2) is the orbital that corresponds to the σ_1*(SiSi) bond orbital. The LUMO+1 (symmetry e) corresponds to the π_1* orbital. The LUMO+2 (symmetry a_1) is a Rydberg orbital, and the LUMO+3 (symmetry a_2) is the σ_2*(SiC) orbital. It is important to note that orbitals σ_1* and σ_2* have interchanged their nature in **2** relative to **1**, **3**, and **4** (Figure 2). This will be highly relevant when we analyze the electronic transitions.

The energy order of the virtual orbitals is the same in **3** and **4**. The LUMO and LUMO+3 (symmetry e) correspond to the π_1* and δ_1* orbitals, respectively. The LUMO+1 and LUMO+2 (symmetry a) correspond to the Rydberg orbital and to the σ_1*(SiC) orbital, respectively.

Electronic Transitions. The vertical excitation energies and oscillator strengths of the first six singlet excited states calculated at the TD-DFT/B3LYP(AC)/cc-pVTZ/cc-pVTZ/6-311G level using the MP2/cc-pVTZ/cc-pVTZ/6-31G** optimized geometries are listed in Table 2, together with available experimental data.[9,12] For **1**, four of the electronic transitions are single electron promotions to valence excited states, and two are single electron promotions to a 4s Rydberg state. For **2**−**4**, five of the electronic transitions are single electron promotions to valence excited states, and only one is a single electron promotion to a 4s Rydberg state.

Transition 1. The lowest energy singlet−singlet electronic transition calculated for **1** lies at 49 000 cm^{-1}, and it is an electronic transition from the ground state to the 2^1A_{1g} excited state. This electronic transition corresponds to a symmetry-forbidden excitation from the σ_1 HOMO to the Rydberg 4s orbital. For disilanes **2**−**4**, the first electronic transition is from the ground state to the 1^1E excited state. It corresponds to an excitation from the σ_1 HOMO to the degenerate π_1* orbital, which is the LUMO+1 in **2** and the LUMO in **3** and **4**. This electronic transition is located at 49 600, 47 400, and 48 200 cm^{-1} in **2**, **3**, and **4**, respectively. The oscillator strength is 0.137, 0.114, and 0.103, respectively. This is the strongest electronic transition in **3** and one of the two strong transitions in **4**.

Transition 2. In **1**, an analogous electronic transition to the 1^1E_u excited state (from the σ_1 HOMO to the degenerate π_1* LUMO+1) is only second in energy and is calculated at 52 100

TABLE 2: TD-DFT Vertical Excitation Energies (E, cm^{-1}) and Oscillator Strengths (f) of Electronic Transitions in Disilanes 1−4

	UV abs (77 K)[a]		UV abs (RT)[a]			TD-DFT[b]		
compound (symmetry)	E	ε_{max}	E	ε_{max}	f	state	E	f
1 (D_{3d})						$2\ ^1A_{1g}$ ($\sigma_1 \rightarrow$ Ryd)	49 000	0[c]
	51 900[d]	9300	52 300	11 600	0.151	$1\ ^1E_u$ ($\sigma_1 \rightarrow \pi_1$*)	52 100	0.145
	61 500[e]					$1\ ^1A_{2u}$ ($\sigma_1 \rightarrow \sigma_1$ *)	57 100	0.093
						$1\ ^1E_g$ ($\pi_1 \rightarrow$ Ryd)	60 600	0[c]
						$2\ ^1E_g$ ($\sigma_1 \rightarrow \delta_1$*)	61 700	0[c]
						$2\ ^1A_{2u}$ ($\pi_1 \rightarrow \pi_1$*)	62 400	0.002
2 (D_3)	48 500(s)	37 000	49 000(s)	38 000	0.223	$1\ ^1E$ ($\sigma_1 \rightarrow \pi_1$*)	49 600	0.137
	52 300	43 800	51 200	45 900	0.589	$1\ ^1A_2$ ($\sigma_1 \rightarrow \sigma_1$ *)	51 500	0.810
						$2\ ^1A_1$ ($\sigma_1 \rightarrow$ Ryd)	52 900	0[c]
						$2\ ^1E$ ($\pi_1 \rightarrow \sigma_1$ *)	53 400	0.058
						$3\ ^1A_1$ ($\pi_1 \rightarrow \pi_1$*)	53 700	0[c]
						$3\ ^1E$ ($\pi_2 \rightarrow \sigma_1$ *)	54 700	0.010
3 (D_3)	48 100	8400	48 400	8900	0.140	$1\ ^1E$ ($\sigma_1 \rightarrow \pi_1$*)	47 400	0.114
						$2\ ^1A_1$ ($\sigma_1 \rightarrow$ Ryd)	49 200	0[c]
						$1\ ^1A_2$ ($\sigma_1 \rightarrow \sigma_1$ *)	51 100	0.022
						$2\ ^1E$ ($\sigma_1 \rightarrow \delta_1$*)	52 500	0.009
						$3\ ^1A_1$ ($\pi_1 \rightarrow \pi_1$*)	55 600	0[c]
						$3\ ^1E$ ($\pi_1 \rightarrow \pi_1$*)	55 800	0.039
4 (C_3)	49 600	7800	48 800	7600	0.138	$1\ ^1E$ ($\sigma_1 \rightarrow \pi_1$*)	48 200	0.103
						$2\ ^1A$ ($\sigma_1 \rightarrow$ Ryd)	50 800	0.00000
						$3\ ^1A$ ($\sigma_1 \rightarrow \sigma_1$ *)	54 300	0.115
						$4\ ^1A$ ($\pi_1 \rightarrow \pi_1$*)	54 800	0.007
						$2\ ^1E$ ($\sigma_1 \rightarrow \delta_1$*)	55 000	0.002
						$3\ ^1E$ ($\pi_1 \rightarrow \pi_1$*)	55 300	0.00001

[a] From ref 12. [b] TD-DFT/B3LYP values calculated using asymptotic correction and cc-pVTZ/cc-pVTZ/6-311G basis set. [c] Transition forbidden by symmetry. [d] In the gas phase, 52 600 cm^{-1} (ref 9). [e] Gas phase (ref 9).

cm^{-1} with an oscillator strength of 0.145, the strongest in this compound. In **2**, the second electronic transition is to the 1^1A_2 excited state, which lies at 51 500 cm^{-1}. It has the highest calculated oscillator strength, 0.810, among all four disilanes analyzed, approximately 6 times higher than the other strong transition in this compound (0.137). It corresponds to an electronic transition from the σ_1 HOMO to the σ_1* LUMO. This is the σ(SiSi)−σ*(SiSi) transition that is considered the most characteristic of oligosilanes and polysilanes. For compounds **3** and **4**, the second electronic transition is to the 2^1A_1 and to the 2^1A excited states, respectively, and it is calculated at 49 200 and 50 800 cm^{-1}, respectively. In **3**, it is symmetry forbidden. Although it is not forbidden in **4**, it has an oscillator strength smaller than 5×10^{-6}. In both compounds, this transition is from the σ_1 HOMO to the 4s Rydberg orbital.

Transition 3. The next calculated electronic transition in **1** lies at 57 100 cm^{-1} and terminates in the 1^1A_{2u} excited state. It has an oscillator strength of 0.093. This electronic transition is a promotion from the σ_1 HOMO to the σ_1* LUMO+2 and can be described as a σ(SiSi)−σ*(SiC) transition. In **2**, the third electronic transition is from the ground state to the 2^1A_1 excited state. It is located at 52 900 cm^{-1}, and it is symmetry forbidden. In **3** and **4**, this electronic transition is of the same nature as in **1**, σ(SiSi)−σ*(SiC), and is an electron promotion from the σ_1 HOMO to the σ_1* LUMO+2. It is located at 51 100 and 54 300 cm^{-1} in **3** and **4**, respectively. It exhibits a relatively small oscillator strength of 0.022 in **3** and 0.115 in **4**.

Transition 4. For all compounds except **3**, the fourth electronic transition involves an electron promotion from the π_1 HOMO−1 degenerate orbital. In **1**, the electronic transition is into the $1\ ^1E_g$ excited state, calculated at 60 600 cm^{-1}. It involves a promotion to the Rydberg 4s orbital and is forbidden by symmetry. For **2**, this electronic transition is into the $2\ ^1E$ excited state and lies at 53 400 cm^{-1}. It has an oscillator strength of 0.058, and the electronic promotion is to the σ_1* LUMO. In **4**, the electronic promotion is to the degenerate π_1* LUMO. This $4\ ^1A$ excited state is located at 54 800 cm^{-1}, and the transition has an oscillator strength of 0.007. In **3**, the fourth electronic transition is to the $2\ ^1E$ excited state. It is calculated at 52 500 cm^{-1} and has an oscillator strength of 0.009. This transition corresponds to a one-electron promotion from the σ_1 HOMO to the degenerate δ_1* LUMO+3.

Transition 5. The fifth calculated electronic transition in **1** lies at 61 700 cm^{-1} and terminates in the $2\ ^1E_g$ excited state. It is a promotion from the σ_1 HOMO to the δ_1* LUMO+3 and is symmetry forbidden. In both **2** and **3**, this transition is to a $3\ ^1A_1$ excited state, calculated at 53 700 and 55 600 cm^{-1}, respectively. It involves an electron promotion from the degenerate π_1 HOMO−1 to the degenerate π_1* orbital, which corresponds to the LUMO+1 in **2** and to the LUMO in **3**. This transition is forbidden by symmetry in both compounds. In **4**, it is of the same nature as in **1**, a promotion from the σ_1 HOMO to the δ_1* LUMO+3. This transition is into the $2\ ^1E$ excited state located at 55 000 cm^{-1} and has a relatively small oscillator strength of 0.002.

Transition 6. The last calculated electronic transition in **1** is to the $2\ ^1A_{2u}$ excited state that lies at 62 400 cm^{-1}. It corresponds to an electron promotion from the π_1 HOMO−1 to the π_1* LUMO+1 and has an oscillator strength of 0.002. In **2**, the electronic transition is into the $3\ ^1E$ excited state located at 54 700 cm^{-1} and has a quite strong oscillator strength of 0.010. It involves an electron promotion from the π_2 HOMO−2 to the σ_1* LUMO. This is the only compound for which we calculate an electronic transition that involves an electron promotion from the HOMO−2. For **3** and **4**, the last calculated transition terminates in the $3\ ^1E$ excited state and is located at 55 800 and at 55 300 cm^{-1}, respectively. For both compounds, it corresponds to an electron promotion from the π_1 HOMO−1 to the π_1* LUMO. The oscillator strength is significant in **3** (0.039) and negligible in **4** (10^{-5}).

Discussion

Molecular Geometries. The optimized minimum energy structures of **1**−**3** are in perfect agreement with the available experimental data[15−17,29] for both bond lengths and bond angles, which gives us confidence in the geometrical parameters calculated for **4**. They also agree with previous MP2/VTZ results,[12] except for the Si−Si bond length of **2**. Our calculation gives a distance of 2.667 Å, in better accord with the experimental value[15] of 2.686 Å than the MP2/VTZ result[12] of 2.74 Å. For unstrained oligosilanes, the VTZ basis set appears to be sufficient.

The maximum difference between experimental and calculated values is 0.019 Å for bond length and 1.7° for bond angles. The most remarkable difference among the four disilanes is the 2.667 Å Si−Si bond length in **2**, which greatly exceeds the standard Si−Si bond length of 2.34−2.35 Å. The disilane **1** shows a more standard Si−Si bond length of 2.356 Å, whereas the SiSi bonds in the propellanes **3** and **4** are shorter than usual, 2.301 and 2.322 Å, respectively. For the Si−C bond lengths, a quite large value of 1.988 Å is found with **2**, and more standard Si−C values of 1.89−1.90 Å with **1**, **3**, and **4**. The variation of the ∠SiSiC bond angle among the disilanes **1**, **2**, and **4** is small, but it decreases significantly, by about 4°, upon going from **1** to **3**, due to the shorter bridges in the tricyclic structure of **3**. The small increase upon going from **1** to **2** indicates that there is about as much steric hindrance among geminal as among the vicinal *tert*-butyl groups in the latter, and the steric problem is mostly accommodated by the amazing stretch of the Si−Si bond to 2.667 Å.

Electronic Spectra. We consider first all electronic transitions in each individual compound and then comment on each important type of transition in the whole group of disilanes.

Hexamethyldisilane (1). The solution UV absorption spectra of **1** recorded in the 42 000−54 000 cm^{-1} range at room temperature (RT) and 77 K contain just one broadband, and the presence of an A term in the MCD spectrum[12] permitted an assignment to a degenerate $\sigma\pi^*$ transition, in agreement with TD-DFT calculations.[12−14] Our vertical excitation energies calculated for **1** (Table 2) also agree with the assignment of this transition to an electron promotion from the σ_1 HOMO to the π_1^* LUMO+1. The solution UV absorption showed a maximum at 51 900 cm^{-1} at 77 K and at 52 300 cm^{-1} at RT, in perfect accord with the calculated 1 ^1E_u state located at 52 100 cm^{-1}. The oscillator strengths calculated at the TD-DFT level and observed at RT also are in excellent agreement, with values of 0.145 and 0.151, respectively.

The gas-phase spectrum of **1** was recorded in the 2100−1200 Å (47 600−83 300 cm^{-1}) range by Harada et al.[9] and contains three clear broad bands, centered at around 1900 Å (52 600 cm^{-1}), 1625 Å (61 500 cm^{-1}), and 1420 Å (70 400 cm^{-1}). Our calculations only include excitation energies up to 62 400 cm^{-1}. They account for the first of these bands, just discussed above. The only other calculated contribution to this band is from the symmetry-forbidden 2 $^1A_{1\ g}$ ($\sigma_1 \rightarrow$4s) Rydberg excitation.

Our results also pertain to the second band, centered at about 1625 Å (61 500 cm^{-1}). It contains contribution from at least three valence excitations into 1 $^1A_{2u}$, 2 ^1E_g, and 2 $^1A_{2u}$ states, and from a Rydberg transition, which involves a one-electron promotion from the π_1 HOMO−1 to the 4s orbital (1 ^1E_g). The main contribution to the onset of the band is due to a transition into the 1 $^1A_{2u}$ state, which is strongly allowed and is calculated at 57 100 cm^{-1}, considerably below the observed peak position at ∼61 500 cm^{-1}. This is an excitation from the σ_1 HOMO to the σ_1^* LUMO+2. The 2 $^1A_{2u}$ ($\pi_1 \rightarrow \pi_1^*$) valence state calculated at 62 400 cm^{-1} also contributes to the observed band, but its oscillator strength is quite small and its effect on the observed band should be almost negligible. This should be even more so for the other two calculated states, 1 ^1E_g and 2 ^1E_g, which are forbidden by symmetry. It appears that in this region the computed excitation energies are no longer reliable.

Hexa-*tert*-butyldisilane (2). Solution UV absorption at RT and 77 K and MCD spectra of **2** were recorded in the 42 000−54 000 cm^{-1} range.[12] At RT, the UV absorption spectrum shows that the first band is a shoulder riding on top of a very broad and much more intense band that starts to rise at lower energies than the first band but peaks at a higher energy, between 52 000 and 53 000 cm^{-1}. Gaussian fitting suggested that the first band peaks at 47 200 cm^{-1} and that there is a much broader and much more intense additional band peaking at 52 800 cm^{-1}. At 77 K, the results were similar, with the first band peaking at 48 200 cm^{-1} and the second at 51 200 cm^{-1}. An LD spectrum was recorded in the 40 000−52 000 cm^{-1} range and showed that the two transitions apparent in the UV spectra are polarized differently.[12] On the basis of these results, the weaker transition was assigned as $\sigma\pi^*$ and the intense one as the $\sigma\sigma^*$. With the present higher quality TD-DFT calculations at hand (Table 2), the results can be confirmed and discussed with increased confidence. The first observed UV absorption band is due to a valence excitation into the 1^1E state, which involves an electron promotion from the σ_1 HOMO to the π_1^* LUMO+1. The agreement between calculated and experimental values is excellent, as the experimental energies are 48 500 and 49 000 cm^{-1} at 77 K and at RT, respectively, and the calculated value is 49 600 cm^{-1}. Also, the theoretical and experimental values of the oscillator strengths are in good agreement, 0.137 and 0.223, respectively. The next band contains a very strong contribution from a valence excitation into the 1 $^1A_2$ state, which involves an electron promotion from the σ_1 HOMO to the σ_1^* LUMO, and it also shows an excellent agreement with the observed UV absorption band at room temperature and at 77 K. The experimental energies are 52 300 and 51 200 cm^{-1} at 77 K and at RT, respectively, and the calculated value is 51 500 cm^{-1}. The theoretical and experimental values of oscillator strengths are in very good accord, 0.810 and 0.589, respectively. The transition moment directions obtained for the first two excited states also agree with the LD spectrum.[12]

Three more electronic transitions, into the 2 $^1A_1$, 2 ^1E, and 3 $^1A_1$ excited states, are calculated in the range of the recorded UV spectra.[12] The excitations to the 2 $^1A_1$ and 3 $^1A_1$ states will not contribute to the overall shape of the band as they are forbidden by symmetry. The 2 ^1E valence state ($\pi_1\sigma_1^*$) that appears at 53 400 cm^{-1}, with an oscillator strength of 0.058, should provide a contribution to the overall shape of the band. However, because the oscillator strength of the transition into the second excited state is so large (0.810), the effect of this state will be almost negligible.

1,6-Disila[4.4.4]propellane (3). Solution UV absorption at RT and 77 K and MCD spectra of **3** were recorded in the 42 000−54 000 cm^{-1} range and showed a very broad band.[12] The LD spectrum was recorded in the 40 000−52 000 cm^{-1} range, and it showed two differently polarized transitions.[12] At the TD-DFT level (Table 2), the observed UV absorption band contains a main contribution from a valence excitation into the 1^1E state. It involves an electron promotion from the σ_1 HOMO to the π_1^* LUMO, and it coincides with the observed UV absorption assigned at room temperature and at 77 K. The agreement between the calculated and experimental values is excellent. The observed energies are 48 100 and 48 400 cm^{-1}at

77 K and at RT, respectively, and the calculated value is 47 400 cm^{-1}. The theoretical and experimental oscillator strengths also are in very good agreement, 0.114 and 0.140, respectively. According to the calculations, the observed band also contains a smaller contribution from a valence excitation into the 1 $^1A_2$ state, which involves an electron promotion from the σ_1 HOMO to the σ_1* LUMO+2 and appears at 51 100 cm^{-1} with an oscillator strength of 0.022. These two contributions agree with the presence of two bands that are polarized differently in the LD spectrum.[12] The excitation into the 2 $^1A_1$ Rydberg state does not contribute to the overall shape of the band, because it is forbidden by symmetry. The last contribution to the broadband observed in the recorded spectra has an almost negligible effect on the overall shape of the band. It arises from the valence excitation into the 2 ^1E state, which involves an electron promotion from the σ_1 HOMO to the δ_1* LUMO+3 that lies at 52 500 cm^{-1} and has an oscillator strength of 0.009.

1,7-Disila[5.5.5]propellane (4). The solution UV absorption at RT and 77 K and the MCD spectrum of **4** were recorded in the 42 000−54 000 cm^{-1} range[12] and showed only one broad band. According to the TD-DFT results (Table 2), the observed UV absorption band contains a strong contribution from a valence excitation into the 1 ^1E valence state, which involves an electron promotion from the σ_1 HOMO to the π_1* LUMO. This electronic excitation is located at 48 200 cm^{-1} and has an oscillator strength of 0.103. The agreement between the calculated and experimental values is again excellent. The observed energies are 49 600 and 48 800 cm^{-1}at 77 K and at RT, respectively, and the calculated value is 48 200 cm^{-1}. Also, the value of 0.103 calculated for the oscillator strength is in very good accord with the experimental value at RT of 0.138. The calculated data also contain a strong contribution from a valence excitation into the 3 ^1A state, which involves an electron promotion from the σ_1 HOMO to the σ_1* LUMO+2 that appears at 54 300 cm^{-1} and carries an oscillator strength of 0.115. The excitation into the 2 ^1A Rydberg state does not contribute significantly to the overall shape of the band.

The Nature of Electronic States of Disilanes. The most prominent low-energy singlet valence excited state of disilanes is the degenerate perpendicular polarized $\sigma\pi$* state, and the parallel polarized $\sigma\sigma$* state occurs at a higher energy. Transitions of both types have been pinpointed by means of MCD and LD spectroscopy in representative members of this class of compounds.[12] The present results are in perfect agreement with the experimental assignments and provide additional confirmation and prediction for as yet unobserved transitions. In **1**−**4**, the $\sigma\pi$* transition is calculated at 52 100, 49 600, 47 400, and 48 200 cm^{-1}, respectively, and the $\sigma\sigma$* transition at 57 100, 51 500, 51 100, and 54 300 cm^{-1}, respectively. The superior numerical agreement of the calculated and observed excitation energies and oscillator strengths is important for confident future applications to larger oligosilanes.

Other types of transitions, such as Rydberg, $\pi\sigma$*, and $\pi\pi$*, have apparently not been detected experimentally with any certainty.

Perhaps most important for an improved understanding of the disilane chromophore itself is the discovery that the first $\sigma\sigma$* state of peralkylated disilanes that have ordinary SiSi bond lengths does not involve excitation into the σ*(SiSi) antibonding orbital but into a σ*(SiC) antibonding orbital. Only in **2**, with its extraordinarily long SiSi bond, is the traditional former assignment correct. This result accounts for the peculiar weakness of the $\sigma\sigma$* transition relative to the $\sigma\pi$* transition in ordinary disilanes, but not in **2**. It is likely that the intense transition of **1** centered at 61 500 cm^{-1} contains contributions from several transitions, including the σ(SiSi)σ*(SiSi) transition, calculated to lie about 4000 cm^{-1} too low, but this region of excitation energies is no longer described reliably by the methods used presently.

The reassignment of the nature of the σ* orbital disagrees with the result of an earlier B3LYP/6-31G* calculation.[12] A series of calculations with various basis sets showed that even a minor improvement leads to the present assignment, and a closer inspection showed that even at the B3LYP/6-31G* level the σ* orbital is of mixed character, with only partial σ*(SiSi) antibonding nature. This means that the usual correlation of the intense first $\sigma\sigma$* transitions in longer alkylated oligosilanes with the first $\sigma\sigma$* transition in a peralkylated disilane is wrong. This has far-reaching consequences, for instance, for attempts to derive parameters for simple models of σ-conjugation in oligosilanes by fitting to experimental excitation energies.[30]

In contrast, in all four disilanes, the standard interpretation of the first $\sigma\pi$* transition is confirmed, and the correlation with the first $\sigma\pi$* transitions of longer oligosilanes remains valid. The much lower intensity that this transition has in oligosilanes than in disilanes is easily understood by reference to the nodal structure of the σ and π* orbitals in oligosilanes with a planar backbone. The former (HOMO) is the least bonding of all σ(SiSi) bonding orbitals and therefore has a node at or near every silicon atom in an oligosilane, with Si(3p) orbitals whose axes are directed along the chain as the main contributors. The latter is the most bonding of all π*(SiC) antibonding orbitals and therefore has no nodes between the contributing Si(3p) atomic orbitals, whose axes are directed perpendicular to the chain. The overlap charge density distribution that results from the multiplication of the two molecular orbitals has dipolar atomic contributions only at chain ends and the rest are quadrupolar. In disilane, the terminal dipoles add in phase, and a reasonable transition dipole moment results for each degenerate component. In longer even-membered oligosilanes, they also add in phase, but the dipolar contributions are small because both orbitals are distributed over the whole molecule. In odd-membered oligosilanes, they add out of phase, and the transition dipole vanishes.

Conclusions

The following conclusions can be drawn.

(i) The MP2/cc-pVTZ/cc-pVTZ/6-31G** geometries of disilanes **1**−**3** are in perfect agreement with experimental data, giving us confidence in the geometry calculated for disilane **4**. This level of calculation is likely to be adequate for longer oligosilanes as well.

(ii) The TD-DFT/B3LYP(AC)/cc-pVTZ/cc-pVTZ/6-311G vertical excitation energies and oscillator strengths of **1**−**4** computed at the optimized geometries are in perfect agreement with experimental data from UV absorption, MCD, and LD spectra of the compounds, up to ∼55 000 cm^{-1}. The method holds considerable promise for the accurate and detailed elucidation of the electronic spectra of longer oligosilanes.

(iii) The results for **1**−**4** confirm and extend the previously proposed assignments and provide detailed insight into their low-energy valence and lowest Rydberg electronic states. The first valence excited state is due to an electron promotion from the σ_1 HOMO to the π_1* orbital, and the second valence excited state corresponds to a promotion from the σ_1 HOMO to the σ_1* orbital for all systems.

(iv) However, in **1**, **3**, and **4**, the terminal σ_1* orbital of the $\sigma\sigma$* transition is not the σ*(SiSi) bond orbital as believed

previously, but a σ^*(SiC) orbital. Only in **2**, which has an exceptionally long SiSi bond, is the traditional assignment correct. This accounts for the strikingly high intensity of the $\sigma_1\sigma_1^*$ transition in **2** as compared to **1**, **3**, and **4**. It is possible that the second band observed in the gas-phase measurement on **1** contains the σ(SiSi)σ^*(SiSi) transition, at a considerably higher energy than originally expected, above the energy range presently addressed.

(v) Because of this reassignment, the first intense $\sigma\sigma^*$ transitions in longer peralkylated oligosilanes do not correlate with the first $\sigma\sigma^*$ transition in ordinary disilanes, as was previously believed.

Acknowledgment. This work was supported by Universitat de València, Generalitat Valenciana, Ministerio de Educación y Ciencia, and the U.S. National Science Foundation (CHE-0446688). NWChem Version 5.0, as developed and distributed by Pacific Northwest National Laboratory, was used to obtain some of these results.

References and Notes

(1) (a) Michl, J.; West, R. In *Silicon-Containing Polymers: The Science and Technology of their Synthesis and Applications*; Jones, R. G., Ando, W., Chojnowski, J., Eds.; Kluwer Academic Publishers: Dordrecht, The Netherlands, 2000; p 499. (b) Fogarty, H. A.; Casher, D. L.; Imhof, R.; Schepers, T.; Rooklin, D. W.; Michl, J. *Pure Appl. Chem.* **2003**, *5*, 999.

(2) Piqueras, M. C.; Crespo, R.; Michl, J. *Mol. Phys.* **2002**, *100*, 747.

(3) Crespo, R.; Merchán, M.; Michl, J. *J. Phys. Chem. A* **2000**, *104*, 8593.

(4) (a) Teramae, H.; Michl, J. *Mol. Cryst. Liq. Cryst.* **1994**, *256*, 149. (b) Albinsson, B.; Teramae, H.; Downing, J. W.; Michl, J. *Chem.-Eur. J.* **1996**, *2*, 529.

(5) (a) Piqueras, M. C.; Merchán, M.; Crespo, R.; Michl, J. *J. Phys. Chem. A* **2002**, *106*, 9868. (b) Piqueras, M. C.; Crespo, R.; Michl, J. *J. Phys. Chem. A* **2003**, *107*, 4661.

(6) (a) Tsuji, H.; Toshimitsu, A.; Tamao, K.; Michl, J. *J. Phys. Chem. A* **2001**, *105*, 10246. (b) Tsuji, H.; Michl, J.; Tamao, K. *J. Organomet. Chem.* **2003**, *685*, 9.

(7) (a) Imhof, R.; Teramae, H.; Michl, J. *Chem. Phys. Lett.* **1997**, *270*, 500. (b) Fogarty, H. A.; Imhof, R.; Michl, J. *Proc. Natl. Acad. Sci. U.S.A.* **2004**, *101*, 10517.

(8) Gilman, H.; Atwell, W. H.; Schwebke, G. L. *J. Organomet. Chem.* **1964**, *2*, 369.

(9) Harada, Y.; Murrell, J. N.; Sheena, H. H. *Chem. Phys. Lett.* **1968**, *1*, 595.

(10) Plitt, H. S.; Balaji, V.; Michl, J. *Chem. Phys. Lett.* **1993**, *213*, 158.

(11) Kishida, H.; Tachibana, H.; Sakurai, K.; Matsumoto, M.; Abe, S.; Tokura, Y. *J. Phys. Soc. Jpn.* **1996**, *65*, 1578.

(12) Casher, D. L.; Tsuji, H.; Sano, A.; Katkevics, M.; Toshimitsu, A.; Tamao, K.; Kubota, M.; Kobayashi, T.; Ottosson, H. C.; David, D. E.; Michl, J. *J. Phys. Chem. A* **2003**, *107*, 3559.

(13) Liu, Z.; Terakura, K.; Abe, S.; Harris, J. F. *J. Chem. Phys.* **1996**, *105*, 8237.

(14) Rooklin, D. W.; Schepers, T.; Raymond-Johansson, M. K.; Michl, J. *Photochem. Photophys. Sci.* **2003**, *2*, 511.

(15) (a) Wiberg, N.; Schuster, H.; Simon, A.; Peters, K. *Angew. Chem., Int. Ed. Engl.* **1986**, *25*, 79. (b) Wiberg, N.; Niedermayer, W.; Noth, H.; Knizek, J.; Ponikwar, W.; Polborn, K. *Z. Naturforsch.* **2000**, *55b*, 389.

(16) Beagley, B.; Monaghan, J. J.; Hewitt, T. G. *J. Mol. Struct.* **1971**, *8*, 401.

(17) Toshimitsu, A.; Katkevics, M.; Sano, A.; Asahara, M.; Yamaguchi, S.; Tamao, K. Presented at the 47th Symposium on Organometallic Chemistry, Nagoya, Japan, 2000;Paper A101, and unpublished results.

(18) Piqueras, M. C.; Michl, J.; Crespo, R. *Mol. Phys.* **2006**, *104*, 1107.

(19) Casida, M. E.; Salahub, D. R. *J. Chem. Phys.* **2000**, *113*, 8918.

(20) Frisch, M. J.; Trucks, G. W.; Schlegel, H. B.; Scuseria, G. E.; Robb, M. A.; Cheeseman, J. R.; Montgomery, J. A., Jr.; Vreven, T.; Kudin, K. N.; Burant, J. C.; Millam, J. M.; Iyengar, S. S.; Tomasi, J.; Barone, V.; Mennucci, B.; Cossi, M.; Scalmani, G.; Rega, N.; Petersson, G. A.; Nakatsuji, H.; Hada, M.; Ehara, M.; Toyota, K.; Fukuda, R.; Hasegawa, J.; Ishida, M.; Nakajima, T.; Honda, Y.; Kitao, O.; Nakai, H.; Klene, M.; Li, X.; Knox, J. E.; Hratchian, H. P.; Cross, J. B.; Bakken, V.; Adamo, C.; Jaramillo, J.; Gomperts, R.; Stratmann, R. E.; Yazyev, O.; Austin, A. J.; Cammi, R. ; Pomelli, C.; Ochterski, J. W.; Ayala, P. Y.; Morokuma, K.; Voth, G. A.; Salvador, P.; Dannenberg, J. J.; Zakrzewski, V. G.; Dapprich, S.; Daniels, A. D.; Strain, M. C.; Farkas, O.; Malick, D. K.; Rabuck, A. D.; Raghavachari, K.; Foresman, J. B.; Ortiz, J. V.; Cui, Q.; Baboul, A. G.; Clifford, S.; Cioslowski, J.; Stefanov, B. B.; Liu, G.; Liashenko, A.; Piskorz, P.; Komaromi, I.; Martin, R. L.; Fox, D. J.; Keith, T.; Al-Laham, M. A.; Peng, C. Y.; Nanayakkara, A.; Challacombe, M.; Gill, P. M. W.; Johnson, B.; Chen, W.; Wong, M. W.; Gonzalez, C.; Pople, J. A. *Gaussian 03*, revision C.02; Gaussian, Inc.: Wallingford, CT, 2004.

(21) Kendall, R. A.; Dunning, T. H., Jr.; Harrison, R. J. *J. Chem. Phys.* **1992**, *96*, 6796.

(22) Hariharan, P. C.; Pople, J. A. *Theor. Chim. Acta* **1973**, *28*, 213.

(23) Becke, A. D. *J. Chem. Phys.* **1993**, *98*, 5648.

(24) Krishnan, R.; Binkley, J. S.; Seeger, R.; Pople, J. A. *J. Chem. Phys.* **1980**, *72*, 650.

(25) Zhan, C.-G.; Nichols, J. A.; Dixon, D. A. *J. Chem. Phys. A* **2003**, *107*, 4184.

(26) Hirata, S.; Zhan, C.-G.; Aprà, E.; Windus, T. L.; Dixon, D. A. *J. Chem. Phys. A* **2003**, *107*, 10154.

(27) Bylaska, E. J.; de Jong, W. A.; Kowalski, K.; Straatsma, T. P.; Valiev, M.; Wang, D.; Aprà, E.; Windus, T. L.; Hirata, S.; Hackler, M. T.; Zhao, Y.; Fan, P.-D.; Harrison, R. J.; Dupuis, M.; Smith, D. M. A.; Nieplocha, J.; Tipparaju, V.; Krishnan, M.; Auer, A. A.; Nooijen, M.; Brown, E.; Cisneros, G.; Fann, G. I.; Früchtl, H.; Garza, J.; Hirao, K.; Kendall, R.; Nichols, J. A.; Tsemekhman, K.; Wolinski, K.; Anchell, J.; Bernholdt, D.; Borowski, P.; Clark, T.; Clerc, D.; Dachsel, H.; Deegan, M.; Dyall, K.; Elwood, D.; Glendening, E.; Gutowski, M.; Hess, A.; Jaffe, J.; Johnson, B.; Ju, J.; Kobayashi, R.; Kutteh, R.; Lin, Z.; Littlefield, R.; Long, X.; Meng, B.; Nakajima, T.; Niu, S.; Pollack, L.; Rosing, M.; Sandrone, G.; Stave, M.; Taylor, H.; Thomas, G.; van Lenthe, J.; Wong, A.; Zhang, A. *NWChem, A Computational Chemistry Package for Parallel Computers, Version 5.0*; Pacific Northwest National Laboratory: Richland, WA 99352-0999, 2006.

(28) Crespo, R.; Piqueras, M. C.; Michl, J. *Theor. Chem. Acc.* **2007**, *118*, 81.

(29) Data from Prof. K. Tamao, Riken Frontier Research System, Tokyo, Japan, private communication.

(30) Schepers, T.; Michl, J. *J. Phys. Org. Chem.* **2002**, *15*, 490.

JP804677V